

Non-traditional thermal behavior of Co(II) coordination networks showing slow magnetic relaxation

Journal:	<i>Inorganic Chemistry Frontiers</i>
Manuscript ID	QI-RES-05-2021-000667.R1
Article Type:	Research Article
Date Submitted by the Author:	15-Jul-2021
Complete List of Authors:	Switlicka, Anna; University of Silesia, Crystallography Machura, Barbara; University of Silesia, Bieńko, Alina; University of Wrocław, Faculty of Chemistry Bieńko, Dariusz; Wrocław University of Technology, Faculty of Chemistry Rajnák, Cyril; University of SS Cyril and Methodius, Department of Chemistry Boca, Roman; University of SS Cyril and Methodius, Department of Chemistry Ozarowski, Andrew; Florida State University, National High Magnetic Field Laboratory Ozerov, Mykhaylo; Florida State University, National High Magnetic Field Laboratory Kozieł, Sandra; University of Wrocław, Faculty of Chemistry

ARTICLE

Non-traditional thermal behavior of Co(II) coordination networks showing slow magnetic relaxation

Received 00th January 20xx,
Accepted 00th January 20xx

Anna Świtlicka^{a*}, Barbara Machura^a, Alina Bieńko^{b*}, Sandra Kozieł^b, Dariusz C. Bieńko^c, Cyril Rajnák^d, Roman Boča^d, Andrew Ozarowski^e and Mykhaylo Ozerov^e

DOI: 10.1039/x0xx00000x

Three new coordination polymers, one-dimensional ones [Co(5,6-(Me)₂-bzim)₂(dca)₂] (**1**), [Co(5-Mebzim)₂(dca)₂]_n (**2**) and two-dimensional polymer [Co(2-Mebzim)(dca)₂]_n (**3**), show DC magnetic data consistent with the $S = 3/2$ spin system with large zero-field splitting $D > 0$, which was confirmed by high-field HF EPR and FIRMS measurements. The experimental spectra of all complexes were simulated with axial g tensor components, a very large positive D value and different E/D ratios. These systems exhibit a slow magnetic relaxation under the moderate DC magnetic field with two relaxation channels. The high-frequency relaxation time develops according to combined Raman and phonon bottleneck relaxation mechanisms resulting from unexpected thermal reciprocating behaviour when the low temperature relaxation time for the HF channel during cooling is shortened.

Introduction

The design and synthesis of coordination polymers (CPs) are of great importance in research of supramolecular and material chemistry due to their diverse structural motifs and potential applications as functional materials in gas storage, adsorption separation, ion exchange, non-linear optics, catalysis, photoluminescence.¹⁻¹⁴ These systems were also found to be good candidates for studying fundamental phenomena in magnetism, including spin canting, metamagnetism, ferromagnetism, antiferromagnetism.¹⁵⁻¹⁹ In addition, some of CPs behave as the Single Chain Magnets (SCMs) or Single Ion Magnets (SIMs), and display slow relaxation of the magnetization.²⁰⁻³⁷

According to Robson's concept, CP networks can be easily generated by using commonly available metal moieties and linking them with linear "spacer" ligands, and their network structures are predominately governed by building blocks abilities to self-assemble.³⁸ In practice, many other factors, including auxiliary ligands, pH value, temperature, solvent polarity, metal salt to ligand ratios, counter ions, must be taken into consideration in the self-assembly process of

coordination polymers of desired network structures. The rational synthesis of these materials still remains a significant challenge.³⁹⁻⁴⁴

One of the most excellent inorganic spacers to construct magnetic coordination polymers is dicyanamide ion (*dca*⁻), displaying multiple bridging coordination modes. In vast majority of polynuclear complexes, *dca*⁻ anion coordinates to a metal centre through two nitrile nitrogen atoms ($\mu_{1,5}$ -*dca*) or one central amide and two nitrile nitrogen atoms ($\mu_{1,3,5}$ -*dca*). The other coordination modes like $\mu_{1,3}$ -*dca*, $\mu_{1,1,5}$ -*dca*, $\mu_{1,1,3,5}$ -*dca*, $\mu_{1,1,5,5}$ -*dca* and $\mu_{1,1,3,5,5}$ -*dca* seem to be far more rare.⁴⁵⁻⁴⁹ With the use of *dca*⁻, it has been possible to obtain numerous CPs with diverse magnetic coupling i.e. ferromagnetism in α -M(*dca*)₂ series of complexes (M = Co or Ni), spin-canted antiferromagnetism (M = Cr, Mn, Fe) and paramagnetism (M = Cu).⁵⁰⁻⁵⁵ Very recently, slow magnetic relaxation phenomena have been confirmed for 2D network of the formula [Co(atz)₂(*dca*)₄], [Co(bim)₂(*dca*)₄] and [Co(bmim)₂(*dca*)₄] (atz = 2-aminotriazine, bim = 1-benzylimidazole, bmim = 1-benzyl-2-methylimidazole), where Co(II) atoms are linked through single $\mu_{1,5}$ -*dca* bridges.⁵⁶⁻⁵⁷

In the present work, which is a part of our effort to explore the magneto-structural relationships in dicyanamide cobalt(II) complexes⁵⁶⁻⁵⁷, three methyl-substituted benzimidazoles differing in the substitution pattern were successfully used for synthesis of dicyanamide Co(II) coordination polymers, and three compounds [Co(5,6-(Me)₂-bzim)₂(*dca*)₂] (**1**), [Co(5-Mebzim)₂(*dca*)₂]_n (**2**) and [Co(2-Mebzim)(*dca*)₂]_n (**3**) (5,6-(Me)₂-bzim = 5,6-dimethylbenzimidazole, 5-Mebzim = 5-methylbenzimidazole, 2-Mebzim = 2-methylbenzimidazole) are reported herein. The coordination polymers **1-3** have been investigated by X-ray diffraction, spectroscopic techniques and variable-temperature magnetic susceptibility measurements,

^a Department of Crystallography, Institute of Chemistry, University of Silesia, 9 Szkolna St., 40-006 Katowice, Poland, E-mail: anna.switlicka@us.edu.pl

^b Faculty of Chemistry, University of Wrocław, 14 F. Joliot-Curie, 50-383 Wrocław, Poland E-mail: alina.bienko@chem.uni.wroc.pl

^c Faculty of Chemistry, Wrocław University of Technology, Wybrzeże Wyspiańskiego 27, 50-370 Wrocław, Poland

^d Department of Chemistry, Faculty of Natural Sciences, University of SS Cyril and Methodius, 917 01 Trnava, Slovakia

^e National High Magnetic Field Laboratory, Florida State University, 1800 East Paul Dirac Drive, Tallahassee, Florida 32310, United States

Electronic Supplementary Information (ESI) available: [experimental section, XRPD spectra, Crystal data and structure refinement and bond lengths [Å] and angles, AC susceptibility. See DOI: 10.1039/x0xx00000x

and their magneto-structural properties have been discussed in relation to the previously reported analogues, especially one-dimensional $[\text{Co}(\text{imidazole})_2(\text{dca})_2]_n$ ⁵⁸⁻⁵⁹ and two-dimensional dicyanamide coordination polymers $[\text{Co}(\text{L})_2(\text{dca})_2]_n$ (L = 2-aminobenzimidazole, 1-benzylimidazole and 1-benzyl-2-methylimidazole).^{56, 60}

Experimental part

Crystal structure determination and refinement

Single crystal X-ray diffraction data of **1–3** were collected on a Gemini A Ultra diffractometer equipped with Atlas CCD detector and graphite monochromated MoK α radiation ($\lambda = 0.71073\text{\AA}$) at room temperature. The unit cell determination

and data integration were carried out using the CrysAlis package of Oxford Diffraction.⁶¹ The structures were solved by direct methods using SHELXS and refined by full-matrix least-squares on F^2 using SHELXL-2014.⁶² All non-hydrogen atoms were refined anisotropically. The hydrogen atoms were placed in calculated positions refined using idealized geometries (riding model) and assigned fixed isotropic displacement parameters, $d(\text{C–H}) = 0.93\text{\AA}$, $U_{\text{iso}}(\text{H}) = 1.2 U_{\text{eq}}(\text{C})$ (for aromatic); and $d(\text{C–H}) = 0.96\text{\AA}$, $U_{\text{iso}}(\text{H}) = 1.5 U_{\text{eq}}(\text{C})$ (for methyl). The methyl groups were allowed to rotate about their local threefold axis. Details of the crystallographic data collection, structural determination, and refinement for **1–3** are given in Table 1, whereas selected bond distances and angles are listed in Table S2.

Table 1. Crystal data and structure refinement for **1–3**

	1	2	3
Empirical formula	C ₂₂ H ₂₀ N ₁₀ Co	C ₂₀ H ₂₂ N ₁₀ Co	C ₂₀ H ₁₆ N ₁₀ Co
Formula weight	483.41	461.40	455.36
T, K	295.0(2)	295.0(2)	295.0(2)
Wavelength, Å	0.71073	0.71073	0.71073
Crystal system	monoclinic	monoclinic	monoclinic
Space group	C2/m	C2/m	P2 ₁ /n
Unit cell dimensions, Å and °			
a	17.196(3)	16.3690(12)	9.1183(7)
b	7.7339(15)	7.3223(4)	8.2739(6)
c	9.988(2)	9.6761(6)	13.2626(9)
α			
β	114.74(3)	113.472(5)	102.821(7)
γ			
V, Å ³	1206.4(5)	1063.80(12)	975.64(13)
Z	2	2	2
D _c , g cm ⁻³	1.331	1.440	1.550
Absorption coefficient, mm ⁻¹	0.741	0.837	0.911
F(000)	498	478	466
Crystal size, mm	0.16 × 0.07 × 0.03	0.32 × 0.17 × 0.04	0.19 × 0.18 × 0.14
θ range for data collection [°]	3.35 to 25.05	3.52 to 25.05	3.49 to 25.05
Index ranges	-19 ≤ h ≤ 20 -9 ≤ k ≤ 9 -11 ≤ l ≤ 11	-19 ≤ h ≤ 19 -8 ≤ k ≤ 8 -11 ≤ l ≤ 10	-8 ≤ h ≤ 10 -8 ≤ k ≤ 9 -15 ≤ l ≤ 15
Reflections collected	4816	4691	3979
Independent reflections	1146 (R _{int} = 0.0246)	1030 (R _{int} = 0.0246)	1721 (R _{int} = 0.0308)
Completeness to 2 θ	99.7	99.6	99.7
Min. and max. transm.	0.719 and 1.000	0.727 and 1.000	0.956 and 1.000
Data / restraints / parameters	1146 / 0 / 97	1030 / 0 / 89	1721 / 0 / 143
Goodness-of-fit on F ²	1.126	1.186	1.081
Final R indices [I > 2 σ (I)]	R ₁ = 0.0254 wR ₂ = 0.0628	R ₁ = 0.0342 wR ₂ = 0.1072	R ₁ = 0.0415 wR ₂ = 0.0713
R indices (all data)	R ₁ = 0.0273 wR ₂ = 0.0643	R ₁ = 0.0376 wR ₂ = 0.1110	R ₁ = 0.0312 wR ₂ = 0.0756
Largest diff. peak and hole, e ⁻ Å ⁻³	0.162 and -0.224	0.309 and -0.421	0.29 and -0.22
CCDC numbers	2085569	2085570	2085571

Magnetic data collection

The DC magnetic data was taken using the SQUID magnetometer (MPMS, Quantum Design) with ca 22 mg of sample. The susceptibility data was acquired at the $B_{DC} = 0.1$ T between $T = 1.8$ and 300 K. This was corrected for the underlying diamagnetism and transformed to the effective magnetic moment. The magnetization data was taken at low temperatures $T = 2.0$ and 5.0 K until $B_{max} = 5.0$ T. No remnant magnetization has been detected. The AC susceptibility data was taken with the same apparatus and the same samples using the amplitude of the oscillating field $B_{AC} = 0.3$ mT. Three regimes were used: (i) scan of the AC susceptibility as a function of the field until $B_{DC} = 0.8$ T at $T = 2.0$ K for a set of four trial frequencies f ; (ii) scan of the AC susceptibility as a function of temperature for 22 frequencies of the oscillating field and a set of temperatures ranging between $T = 1.8$ and 7.0 (8.0) K, all at the properly selected field $B_{DC} = 0.2$ (0.15) T. (iii) This dataset has been rearranged to the functions $\chi' = F_r(f, T, [B_{DC}])$ and $\chi'' = F_i(f, T, [B_{DC}])$.

All data handling and fitting has been done by exploiting the software MIF&FIT.⁷⁶ The DC susceptibility and magnetization data was fitted simultaneously using the spin Hamiltonian

$$\hat{H}_a = D(\hat{S}_z^2 - \hat{S}^2 / 3)\hbar^{-2} + B\mu_B\hbar^{-1}(g_z\hat{S}_z \cos\theta_a + g_x\hat{S}_x \sin\theta_a) \quad (1)$$

where D – axial zero-field splitting parameter, θ_a – the polar angle for a number $N = 11$ grids distributed uniformly over half of the meridian. The eigenvalues enter the partition functions from which the susceptibility and/or magnetization are obtained by the apparatus of statistical thermodynamics, and then averaged over a -points.

The AC susceptibility data has been fitted by employing the two-set Debye model

$$\chi(\omega) = \chi_s + \frac{\chi_{T1} - \chi_s}{1 + (i\omega\tau_1)^{1-\alpha_1}} + \frac{\chi_{T2} - \chi_{T1}}{1 + (i\omega\tau_2)^{1-\alpha_2}} \quad (2)$$

giving rise to the adiabatic susceptibility χ_s , and two sets of isothermal susceptibilities χ_{T1} and χ_{T2} , distribution parameters α_1 and α_2 , and relaxation times τ_1 and τ_2 referring to the maxima of the primitive Debye-like curves that merge to a registered envelope ($\omega = 2\pi f$). Closed formulae for the dispersion χ' and absorption χ'' are available so that the fitting procedure is fast. In fact, the joint functional $F = w \cdot E(\chi') + (1-w) \cdot E(\chi'')$ constructed of relative errors is subjected to a non-linear minimization.

HF-EPR and Far-Infrared Magnetic Spectroscopy (FIRMS) studies

Far Infrared Magnetic Spectroscopy was performed at the National High Magnetic Field Laboratory on a 17 T vertical-bore superconducting magnet coupled with a Fourier-transform infrared spectrometer Bruker Vertex. The experimental set-up was equipped by a mercury lamp and a composite silicon bolometer (Infrared Laboratories), as a THz radiation source and detector, respectively. The THz radiation

was guided inside an evacuated (~ 4 mBar) optical beamline to the top of the lightpipe probe holding the sample, which is an eicosane pellet containing ~ 4 mg of the studied compound. The intensity of the transmitted THz radiation was measured in the spectral region between 18 and 730 cm^{-1} (0.55–22 THz) with the resolution of 0.3 cm^{-1} (9 GHz). Both sample and bolometer were cooled by a low-pressure helium gas to the temperature of 5 K. High-frequency EPR spectra were recorded on the 17 T transmission instrument of the EMR facility. The instrument is equipped with a superconducting magnet (Oxford Instruments) capable of reaching a field of 17 T. Microwave frequencies over the range 52–630 GHz were generated by a phase-locked Virginia Diodes source, producing a base frequency of 8–20 GHz, which was multiplied by a cascade of frequency multipliers. The instrument is a transmission-type device and uses no resonance cavity.⁶³ The high-field EPR spectra were simulated using computer programs written by one of us.⁶⁴

Results and discussion

Synthesis, spectroscopic and thermal characterization

X-ray quality crystals of **1–3** were grown by slow evaporation of the mother liquor at room temperature. The phase purity of the compounds has been verified by powder diffraction measurements. As shown in Figures S1–S3, the XRPD patterns measured for the polycrystalline samples are in nice agreement with the powder pattern simulated from the respective single crystal X-ray data using Mercury 3.0.

The IR analyses of cobalt(II) compounds indicate the presence of dicyanamide moiety and monodentate N-donor ligands (Figures S4–S6). Spectra of **1–3** show intense absorption bands $\nu_s(\text{C}\equiv\text{N})$ at 2177–2187 cm^{-1} and $\nu_{as} + \nu_s(\text{C}\equiv\text{N})$ and $\nu_{as}(\text{C}\equiv\text{N})$ in the range 2274–2277 cm^{-1} and 2248–2253 cm^{-1} , respectively. The shift toward higher frequencies compared with these of free dca^- anion (2286, 2232, 2169 cm^{-1}) confirmed coordination of the dca^- in the cobalt(II) compounds.^{65–66} Peaks revealing the presence of benzimidazole derivatives occur in the ranges 3203–3368 cm^{-1} (N–H stretching vibrations) and 1312–1534 cm^{-1} ($\nu(\text{C}=\text{N})$ and $\nu(\text{C}=\text{C})$).

The UV-Vis-NIR solid reflectance spectra of **1–3** are shown in Figure S7, while the electronic spectral data of **1–3** are summarized in Table S1. The solid reflectance spectra of **1–3** show $d-d$ transitions in the visible and NIR regions centered at 1064 nm (9398 cm^{-1}), 546 nm (18315 cm^{-1}) and 494 nm (20242 cm^{-1}) for **1**, 1056 nm (9469 cm^{-1}), (18348 cm^{-1}) and 499 nm (20040 cm^{-1}) for **2** and 1079 nm (9267 cm^{-1}), 543 nm (18416 cm^{-1}) and 481 nm (20790 cm^{-1}) for **3**. These bands can be assigned to the spin allowed electronic transitions in d^7 high-spin octahedral ligand field ${}^4\text{T}_{1g}(\text{F}) \rightarrow {}^4\text{T}_{2g}(\text{F})$, ${}^4\text{T}_{1g} \rightarrow {}^4\text{A}_{2g}(\text{F})$ and ${}^4\text{T}_{1g}(\text{F}) \rightarrow {}^4\text{T}_{1g}(\text{P})$.⁶⁷ The high energy absorptions are characteristic for $n(\text{non-bonding}) \rightarrow \pi^*$ and $\pi \rightarrow \pi^*$ transitions of the organic ligand. The ligand field parameters were calculated from the energy data of the $d-d$ transitions through the equations $Dq = \frac{1}{10}(\nu_2 - \nu_1)$ and $B = \frac{1}{15}(\nu_3 + \nu_2 - 3\nu_1)$. The values

of the parameters Dq and B equal 892 cm^{-1} and 691 cm^{-1} for **1**, 888 cm^{-1} and 665 cm^{-1} for **2**, 915 cm^{-1} and 760 cm^{-1} for **3**, which are typical for six-coordinate cobalt(II) ions in an octahedral environment.⁶⁸⁻⁶⁹

Description of the structures

Structures of $[\text{Co}(\text{5,6-(Me)}_2\text{-bzim})_2(\text{dca})_2]$ (**1**) and $[\text{Co}(\text{5-Mebzim})_2(\text{dca})_2]_n$ (**2**)

The X-ray diffraction studies revealed that structures **1** and **2** adopt infinite chain propagated along b axis (Figures 1a and 2b). The coordination environment of Co(II) atoms, located at the special Wyckoff position c (in **1**) and a (in **2**) of $C2/m$ space group, is determined by two axially coordinated N-donor ligands in *trans* position (5,6-(Me)₂-bzim in **1** and 5-Mebzim in **2**) and nitrogen atoms from four dicyanamide groups occupying equatorial plane. The equatorial bond lengths [Co(1)–N(99) = $2.1981(14)\text{ \AA}$ in (**1**) and $2.141(2)\text{ \AA}$ in (**2**)] are longer than the axial Co–N_L bond distances [Co(1)–N(1) = $2.1165(19)\text{ \AA}$ in (**1**) and $2.122(3)\text{ \AA}$ in (**2**)], in analogy to $[\text{Co}(\text{L1})(\text{dca})_n(\text{PF}_6)_n]$,⁶⁸ $[\text{Co}(\text{im})_2(\text{dca})_2]_n$,⁵⁸ and $[\text{Co}(\text{L3})_2(\text{dca})_2]_n$,⁶⁹ where L1= N,N'-bis(2-pyridinylbenzylidene)ethane-1,2-diamine, im= imidazole and mepy = 4-methylpyridine (Table S5).⁷²⁻⁷⁴

The neighbouring Co(II) ions are doubly bridged by $\mu_{1,5}$ -dca ions to form 12-membered ring $\text{Co}(\mu_{1,5}\text{-dca})_2\text{Co}$. The Co–N–C angles in the $\text{Co}(\mu_{1,5}\text{-dca})_2\text{Co}$ cycle significantly depart from linearity [$161.49(12)^\circ$ in **1** and $160.41(19)^\circ$ in **2**]. The dicyanamide linkers are angular with C–N–C angles $120.20(18)^\circ$ in **1** and $117.8(3)^\circ$ in **2** and close to linear N–C–N units with angles equal $175.43(15)^\circ$ in **1** and $175.1(2)^\circ$ in **2**. The shortest Co \cdots Co distance spanned by the dca^- of $7.734(1)\text{ \AA}$ in **1** [Co \cdots Co^(h); (h) = x, -1+y,z] is longer compared to $7.322(3)\text{ \AA}$ in **2** [Co \cdots Co⁽ⁱ⁾; (i) = x, 1+y,z] and 7.359 \AA [Co \cdots Co^(j); (j) = x, y, -1+z] in $[\text{Co}(\text{imidazole})_2(\text{dca})_2]_n$,⁵⁸⁻⁵⁹ which is attributed to introduction of the more sterically hindered 5,6-(Me)₂-bzim. In similarity to $[\text{Co}(\text{imidazole})_2(\text{dca})_2]_n$, the chains of **1** and **2** are linked by N(2)–H(2) \cdots N(98) hydrogen bonds into supramolecular two-dimensional network [$2.979(3)\text{ \AA}$, D–H \cdots A= 169.0° ; (k): $1/2+x, 1/2+y, z$ in **1** and $2.983(5)\text{ \AA}$, D–H \cdots A= 159.0° ; (l): $1/2-x, 1/2+y, z$ in **2**] (see Figures 1b, 2b). The striking difference between them concerns the closest interchain separations, which are significantly longer for **1** ($9.428(1)\text{ \AA}$) and **2** ($8.966(1)\text{ \AA}$) relative to $[\text{Co}(\text{imidazole})_2(\text{dca})_2]_n$ ($6.567(5)\text{ \AA}$).

Structure of $[\text{Co}(\text{2-Mebzim})(\text{dca})_2]_n$ (**3**)

In the complex **3**, cobalt(II) ions occupy a special Wyckoff position d of $P2_1/n$ space group with multiplicity two. The asymmetric unit consists of dicyanamide ion and molecule of monodentate ligand (2-Mebzim) bound to Co(II) center (Figure 3a). The single X-ray analysis of $[\text{Co}(\text{2-Mebzim})(\text{dca})_2]_n$ revealed that dca^- groups join the Co(II) atoms into rhombus-grid sheets, which are further interlinked into a supramolecular 3D structure through hydrogen bonds N(2)–H(2) \cdots N(98)(m) [$3.104(3)\text{ \AA}$, D–H \cdots A= 149.0° (m): $1/2+x, 1/2-y, 1/2+z$] and C(2)–H(8C) \cdots N(99) [$3.353(3)\text{ \AA}$, D–H \cdots A= 144.0°] (Figure 3).

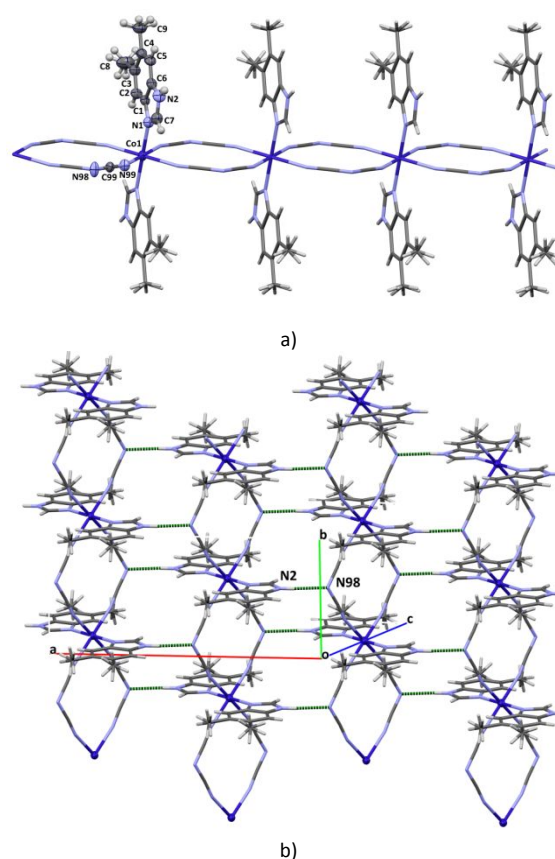


Figure 1. a) One-dimensional structure of **1** formed by double $\mu_{1,5}$ -dca bridges together with atom numbering; b) View of the fragment of supramolecular 2D network generated through N–H \cdots N interactions.

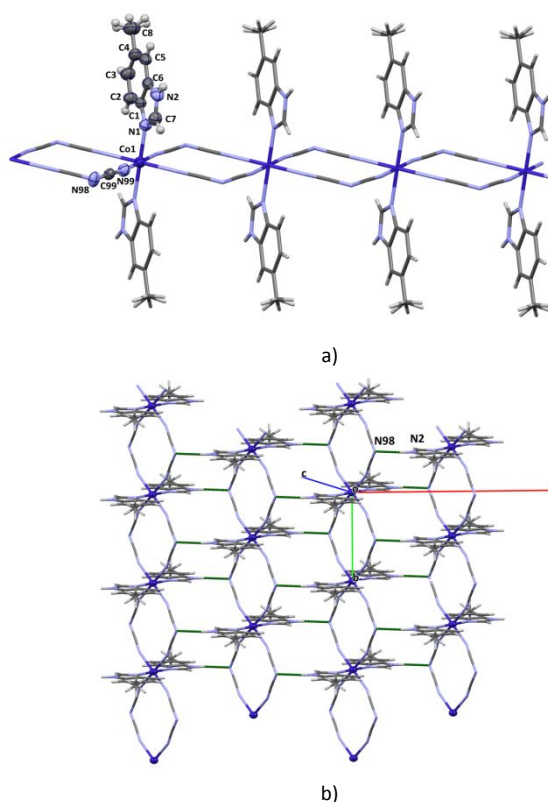


Figure 2. a) One-dimensional coordination network of **2** formed by double $\mu_{1,5}$ -dca bridges together with atom numbering; b) View of the fragment of supramolecular 2D network generated through N–H \cdots N interactions.

The shortest intralayer Co \cdots Co separation through dca $^-$ linkers is 8.273(9) Å, the metal-metal distances through diagonals are equal 14.331(1) and 8.273(9) Å, while interlayer Co \cdots Co distances is equal 9.118(3) Å. Each cobalt(II) atom exists in the slightly elongated octahedral coordination environment defined by two nitrogen atom of 2-Mebzim molecules at axial positions [Co(1)–N(1)=2.1513(18) Å] and four nitrile atoms at equatorial sites [Co(1)–N(97)=2.1445(19) Å; Co(1)–N(99)=2.1405(19) Å] (Table S3, ESI). Like in the complexes **1** and **2**, the dicyanamide are angular with the C–N–C angles of 119.7(2) $^\circ$ and close to linear N–C–N with angles equal 173.2(2) $^\circ$ and 173.4(2) $^\circ$, and the Co–N–C significantly depart from linearity [C(98)–N(97)–Co(1)=151.16(18) $^\circ$; C(99)–N(99)–Co(1)=160.73(19) $^\circ$]. The four single $\mu_{-1,5}$ -dca ligands bridge the cobalt atoms into 4-c unital net described by the {4 4 .6 2 } Schläfli symbol and a [4.4.4.4.6(2).6(2)] extended point symbol, which corresponds to *sql* topological type.⁷⁵ This topology was also confirmed for the related dicyanamide Co(II)

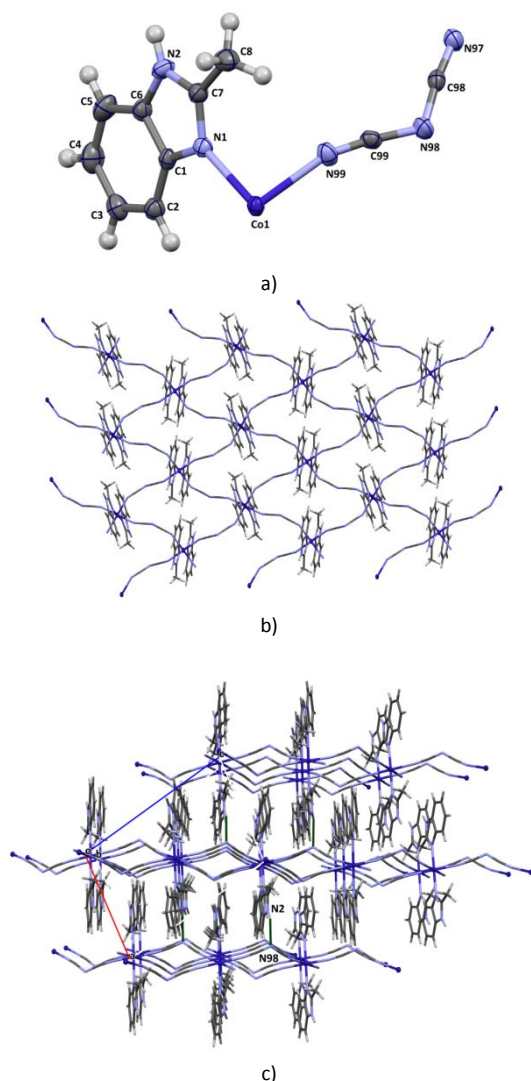


Figure 3. a) Perspective view of the asymmetric unit of **3** showing the atom numbering. Displacement ellipsoids are drawn at 50% probability; b) Two-dimensional coordination network of **3** formed by $\mu_{1,5}$ -dca bridges; c) View of a fragment of supramolecular 3D structure generate through C–H \cdots N interactions.

coordination polymers [Co(L) $_2$ (dca) $_2$] $_n$ bearing benzimidazole and its 2-substituted derivatives as well as N-substituted imidazoles. Depending on imidazole-based ligand, these networks differ in Co \cdots Co separations through the dca $^-$ and metal–metal distances through the diagonals, forming square or rhombus sheets (Table S6). Replacing benzimidazole by 2-Mebzim leads to significant elongation Co \cdots Co separation through dca $^-$ linkers (Table S6).

The HF-EPR and FIRMS spectra

The HF-EPR spectra of **1** exhibit three transitions whose effective g-values are frequency-independent and equal 6.93, 2.94 and 1.94 (Figure S8). This is a characteristic picture of hexa-coordinated high-spin Co(II) with very large zero-field splitting. It is not possible to determine the spin Hamiltonian D and E parameters from HF-EPR spectra, as only the intra-Kramers transitions are observed.

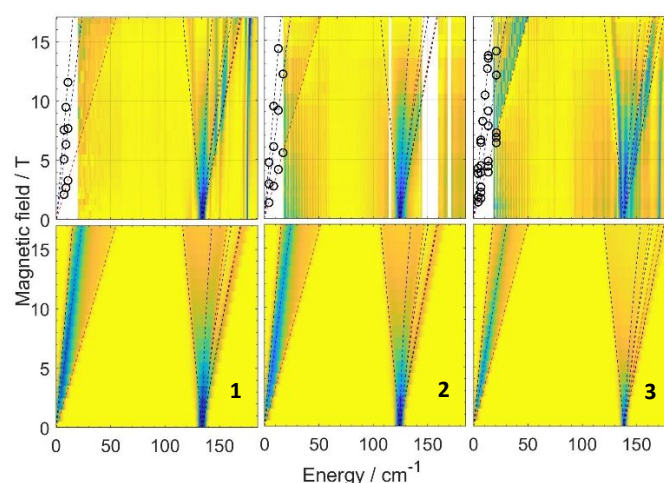


Figure 4. (Top) FIRMS spectra for **1**, **2** and **3** measured in powder sample at 5 K.

The color trend from blue to yellow corresponds to a decrease of the magnetic resonance absorption. Zero-field transitions for **1**, **2** and **3** are clearly visible at 134, 124 and 138 cm^{-1} , respectively, representing the transition between the $\pm 1/2$ and $\pm 3/2$ Kramers doublets. The intra-Kramers transitions within the $\pm 1/2$ manifold is also visible at higher fields (10 – 17 T) in the low-energy region (20 – 50 cm^{-1}), and are in excellent agreement with HF-EPR data, shown by circles. The white regions correspond to spectral ranges without reliable data. (Bottom) Simulated intensity of the magnetic absorptions for the powder sample of **1**, **2** and **3**, respectively. The simulations were done for $S=3/2$ Spin Hamiltonian by Easyspin package⁷⁷ and parameters mentioned in the text. The dashed guidelines show resonances in single crystal for magnetic field applied along x,y,z-direction of the D tensor (including those of nominally forbidden transitions). Therefore, the FIRMS measurements were performed. In FIRMS, a sweep at terahertz frequencies is applied to a system and transmission is measured as a function of frequency. Typically, the raw transmission spectrum is very rich for spectroscopic features. To recognize the transitions of magnetic origin, many

frequency-swept spectra are recorded at different magnetic fields. The FIRMS spectrum is obtained after the normalization of each spectrum by the reference, which is the average transmission spectrum for all magnetic fields. Hence, the FIRMS spectrum picks out solely field-dependent spectral features among the rich field-independent spectral features, such as vibrational modes and instrumentation response. The FIRMS spectrum of **1** (Figure 4) shows a zero-field transition at 134.0 cm^{-1} , which represents the splitting between the $m_s = \pm 1/2$ and $m_s = \pm 3/2$ Kramers doublets. The magnitude of this splitting equals

$$\Delta = 2\sqrt{D^2 + 3E^2} \quad (3)$$

When neglecting the E parameter, $|D/hc|$ equals 68.5 cm^{-1} , in an agreement with the magnetic data fitting results (below). The effective g values in such cases depend on the real g values and the E/D ratio. When trying to reproduce these g_{eff} values by changing the E/D ratio while keeping Δ constant at 67 cm^{-1} , and assuming $g_x = g_y$, one arrives at $D = 62.5\text{ cm}^{-1}$, $E = 17.5\text{ cm}^{-1}$, $g_x = g_y = 2.62$, $g_z = 2.48$. These values were obtained by simulating of powder HF-EPR and FIRMS spectra, using $S=3/2$ spin Hamiltonian and Easyspin package.⁷⁷ The HF-EPR spectra of **2** exhibit three transitions whose frequency-independent effective g values are very similar to those of **1** – 6.65, 3.02 and 1.92 (Figure S8). Also, the splitting between the Kramers doublets seen in the FIRMS spectra is 124 cm^{-1} , close to that observed for **1**. The simulation of the FIRMS spectra gives a good agreement with the experimental data using parameters: $D = 60\text{ cm}^{-1}$, $E = 9\text{ cm}^{-1}$, $g_x = g_y = 2.62$, $g_z = 2.48$.

In the FIRMS spectra of **3**, there are multiple zero-field transitions around 138 cm^{-1} , which is not possible in an $S = 3/2$ system. The simulation using spin-Hamiltonian for single $S=3/2$ and parameters $D = 67\text{ cm}^{-1}$, $E = 10\text{ cm}^{-1}$, $g_x = g_y = 2.62$, $g_z = 2.48$ revealed a fair agreement with an experimental data. Too many transitions are also seen in HF-EPR spectra indicating either the presence of multiple species or metal-metal interactions (Figure S9)

DC magnetic data

The DC magnetic data (temperature evolution of the effective magnetic moment, and the field dependence of the magnetization per formula unit) is displayed in Figure 5. The room-temperature effective magnetic moment adopts values of $\mu_{\text{eff}} = 4.83$, 4.91 , and $4.90\ \mu_{\text{B}}$, for **1** through **3** respectively; these values are typical for the high-spin mononuclear Co(II) complexes with $S = 3/2$ and $g_{\text{av}} \sim 2.5$. On cooling, the effective magnetic moment stays almost constant down to ca 100 K and then gradually decreases. This feature indicates a presence of the significant zero-field splitting. Also the magnetization curves do not saturate to a spin-free value of $M_{\text{sat}} \sim g_{\text{av}}S$ which again indicates the presence of the zero-field splitting. The fitting of the DC magnetic data gave the spin-Hamiltonian parameters as listed in Table 2. Two additional corrections were made: temperature-independent magnetism χ_{TIM} , and the molecular-field correction (zj). The fitting is acceptable, though not perfect. Notice, the real systems are 1D or 2D networks with some (small) exchange interaction of the

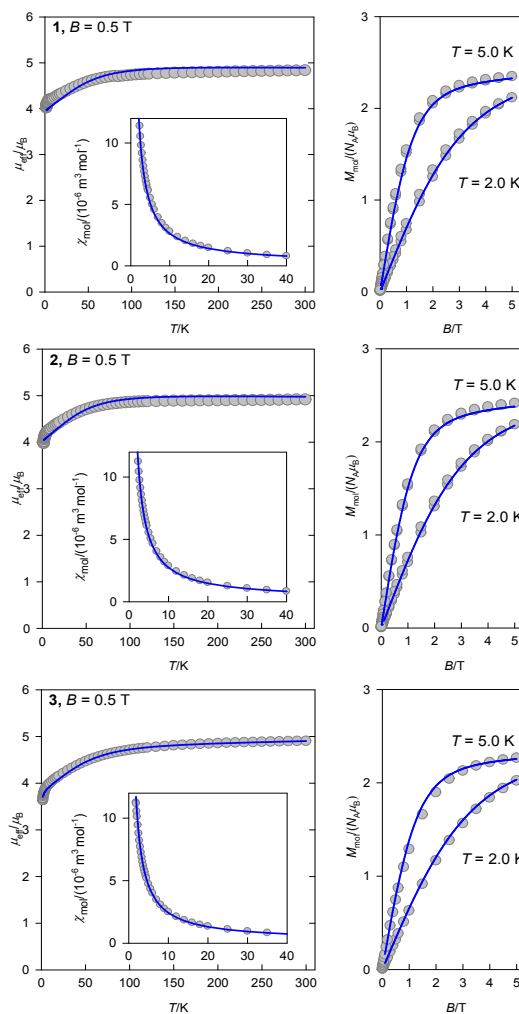


Figure 5. DC magnetic data for **1**, **2**, and **3**: left – temperature evolution of the effective magnetic moment (inset: molar magnetic susceptibility in SI units); right – field dependence of the magnetization per formula unit. Solid lines – fitted.

Table 2. Spin Hamiltonian parameters extracted from the DC magnetic data

	1	2	3
$D/hc / \text{cm}^{-1}$	63(19)	60(8)	65(20)
g_z	2.0	2.0	2.0
g_{xy}	2.73(2)	2.78(1)	2.63(2)
$\chi_{\text{TIM}} / 10^{-9} \text{ m}^3 \text{ mol}^{-1}$	0	0	7.5
$zj/hc / \text{cm}^{-1}$	0	0	-0.02
$ D/hc / \text{cm}^{-1}$ (EPR) ^a	67	62	~ 69

^a Rhombic ZFS parameter E is omitted.

antiferromagnetic nature. Moreover, there might be also the zero-field splitting parameter E in the play.

There is a conceptual problem for the hexacoordinate Co(II) complexes: the octahedral mother electronic term $^4T_{1g}$ on symmetry lowering to D_{4h} splits into the $^4A_{1g}$ and 4E_g daughter terms. The former applies in the case of a compressed tetragonal bipyramid and in such a case the spin-Hamiltonian concept is fully applicable giving rise to $D > 0$ and $g_z = 2.0$ as necessary constraints.⁷⁸ This is the case of **1** and **2**. In the opposite distortion to the elongated tetragonal bipyramid (like for **3**) the orbitally degenerate term 4E_g causes that the spin-

Hamiltonian concept fails and the D-parameter is undefined unless an orthorhombic distortion applies. This complicates the analysis of the DC magnetic data and also the FIRMS data. In such a case the Griffith-Figgis model Hamiltonian is more appropriate for the magnetic data analysis and it could explain an extra energy gap registered by FIRMS at 230 cm^{-1} beyond the spin-Hamiltonian limit⁷⁸

AC susceptibility data

The first scan of the AC susceptibility is displayed in Figure 6 - left. At the zero magnetic field the out-of-phase component χ'' is zero so that the complexes under study are not natural single ion magnets. However, with the increasing DC magnetic field the absorption curves increase until a maximum and then attenuate. The profiles of $\chi'' = F_i(B, f, [T])$ curves depend upon the individual frequencies. At low fields $B_{\text{DC}} \sim 0.2$ T the response culminates for higher frequencies $f \sim 111 - 1116$ Hz; at the higher field this mode is suppressed and the response culminates at low frequencies $f \sim 1 - 11$ Hz.

The second scan of the AC susceptibility refers to a temperature dependence in a selected DC field for a set of 22

frequencies ranging between $f = 0.1 - 1500$ Hz (Figure S9). The same dataset has been rearranged in order to get the frequency dependence as displayed in Figure 6 - right (only χ'' is displayed there).

The Arrhenius-like plot for the high-frequency relaxation time $\tau(\text{HF})$ shows no indication of the quantum tunnelling of magnetization since it is temperature dependent event at the lowest edge of the data taking $T = 1.8$ K (Figure 6 - left). Notice, a positive value of the axial zero-field splitting parameter D discriminates the presence of the Orbach (through-barrier) relaxation mechanism so that one is left with the Raman-like processes with $\tau^{-1} \sim T^n$ dependence. A single Raman-like term, however, is incapable of reproducing the whole data set. Therefore two such terms have been probed *via* eqn $\tau^{-1} = CT^n + FT^l$ that is strongly supported by Figure 6 - right where three data points at the lowest and the highest temperature edge follow a linear relationship $\ln \tau = b_0 - b_1 \ln T$. The coefficients $b_1 = n$ and l were used as a first trial for the non-linear optimization that finally gave the relaxation parameters listed in Table 3.

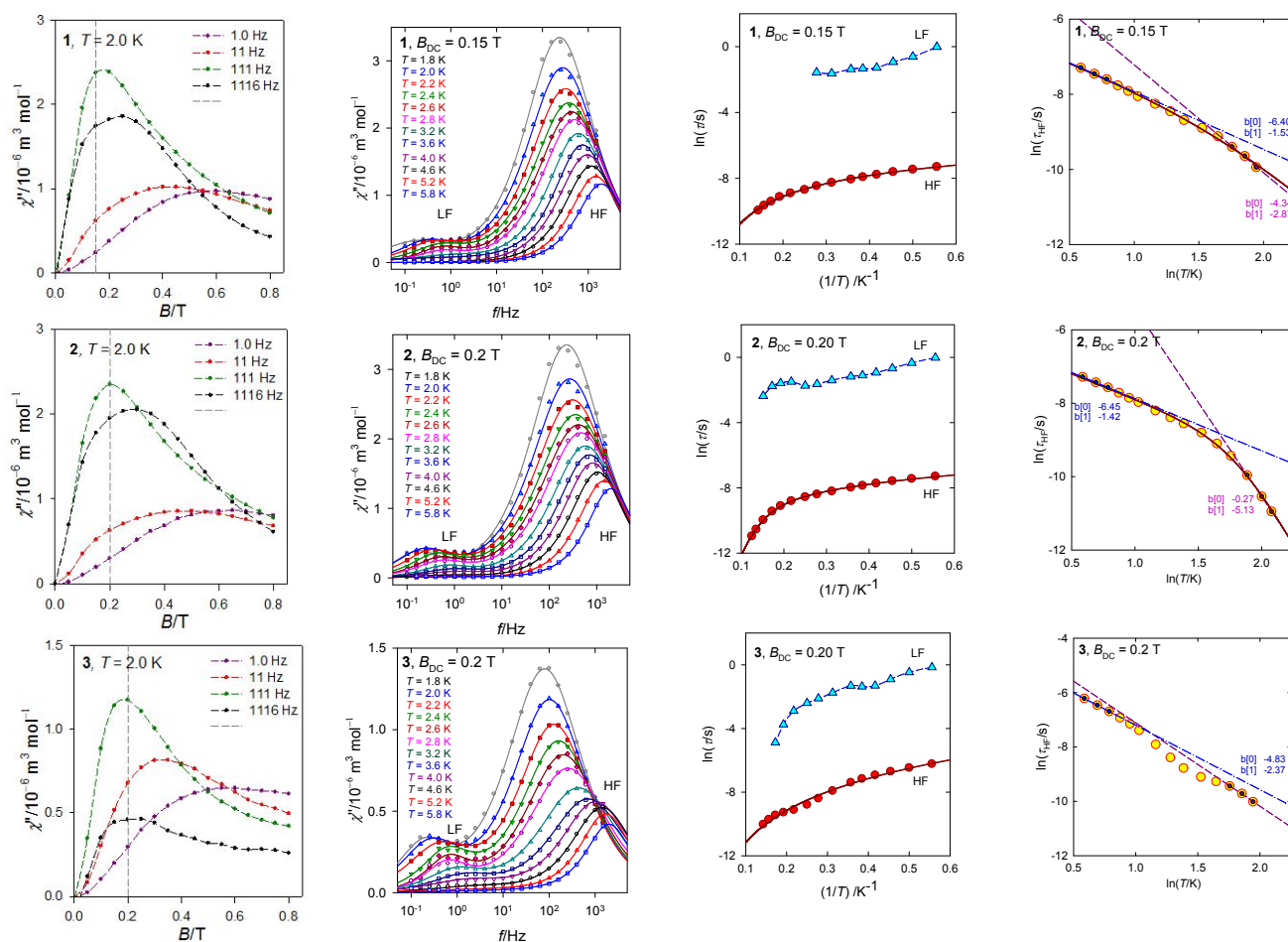


Figure 6. Left panels: field dependence of the out-of-phase susceptibility for **1** through **3** at $T = 2.0$ K for a set of trial frequencies. Lines – guide for eyes. A horizontal bar indicates the field selected for subsequent studies. Right panels: frequency dependence of the out-of-phase susceptibility for **1** through **3** at the fixed B_{DC} . Lines – fitted, using the two-set Debye model.

Figure 7. Left panels: Arrhenius-like plots for **1** through **3**. Solid line – fitted with Raman-like and phonon-bottleneck terms $\tau^{-1} = CT^n + FT^l$. LF (HF) – low frequency (high frequency) relaxation channel. Right panels: temperature dependence of the high-frequency relaxation time for **1** through **3**. Dashed (dot-dashed) lines – linear fits to the high-temperature (low-temperature) windows. Solid – combined Raman-like and phonon-bottleneck terms.

This set of the relaxation parameters generates a line that passes through experimental points. (Some anomaly is seen in Figure 7 - right for **3**.)

Table 3. Relaxation parameters extracted from the AC susceptibility data ^a

	1	2	3
$C / s^{-1} K^n$	16	$89(74) \times 10^{-3}$	90(10)
n	3.3(12)	6.3(4)	2.39(9)
$F / s^{-1} K^l$	625(68)	673(46)	
l	1.36(43)	1.37(8)	

^a Equation $\tau^{-1} = CT^n + FT^l$

Theory of the phonon bottleneck effect has old roots ⁷⁹⁻⁸¹ and it was applied mostly to the lanthanide salts. There are recent reports about the presence of the phonon bottleneck effect also in transition metal and lanthanide complexes showing slow magnetic relaxation.^{82,83} Recently, an anomalous "reciprocating thermal behaviour" has been discovered having its origin in the phonon bottleneck effect.⁸⁴⁻⁸⁶

The dynamic magnetic properties of three complexes under study can be also compared to analogous systems possessing hexacoordinated Co(II) ion. Many examples of such complexes presented in literature exhibit SMM or SIMs behaviour with one or two (sometimes three) relaxation modes and effective energy barriers for spin reversal typically in the range of 20 – 50K. Unlike these systems, complexes **1** to **3** are rather rare example of 1-D coordination polymer based SIM. ⁸⁷⁻⁸⁸ Widely separated Co(II) ions and the poor ability of mediate exchange through the double $\mu_{1,5}$ -dca bridge was attributed to the minimized magnetic interaction between the magnetic centres connected by long ligands account for the magnetic isolation. Observed two relaxation modes were attributed to the existence of intermolecular interactions (hydrogen bonds, π - π stacking, H- π interactions) typical for these systems with aromatic ring which can form at low temperature aggregates such as dimers or finite chains, disintegrated on heating. The HF relaxation channel is ascribed to the single centres whereas LF (IF) modes to some aggregates relaxing more slowly. Usually the high-frequency relaxation time obeys the predictable temperature dependence. However, complexes **1** to **3** present examples of a non-traditional thermal behaviour when at the low temperature the relaxation time, referring to the high-frequency relaxation channel, is shortened on further cooling instead of an expected prolongation.

Conclusions

This work, together with the previously reported results, provided an opportunity to discuss the impact of structural modification of the bezimidazole auxiliary ligands on the coordination networks of Co-dca systems. The combination of 2-methylbenzimidazole with cobalt(II) salt and $\text{NaN}(\text{CN})_2$ led to formation of $[\text{Co}(\text{2-Mebzim})(\text{dca})_2]_n$ displaying 2D coordination network formed by rhombus-grid sheets interlinked by hydrogen bonds N-H...N. On contrary, the use of 5,6-(Me)₂-bzim and 5-Mebzim resulted in formation compounds adopting adopt infinite chain $[\text{Co}(\text{L})_2(\text{dca})_2]$ structures with

inter- and intra-chain Co...Co separations influenced by methyl substitution pattern.

All three compounds show DC magnetic data consistent with the $S = 3/2$ spin system with large zero-field splitting D . These systems exhibit a slow magnetic relaxation under the moderate DC magnetic field. The fitting of the AC magnetic susceptibility to the two-set Debye model allows determining the relaxation parameters; the high-frequency relaxation time develops in match with a combined Raman and phonon bottleneck relaxation mechanisms.

The obtained result confirm also that the design of SIMs may be achieved by organizing magnetic ions with suitable local magnetic anisotropy into polymeric architectures, which could be considered as a promising approach for a new generation of molecular magnetic materials.

Acknowledgements

The magnetic measurements were supported by University of Wroclaw program IDUB (BPIDUB. 4610.17.2021.KP.B) (A.B.) The National High Magnetic Field Laboratory is supported by National Science Foundation Cooperative Agreement No. DMR-1644779 (A.O. and M.O) and the State of Florida. Slovak grant agencies (APVV 18-0016, VEGA 1/0086/21) are acknowledged for the financial support. (R.B)

Supporting information

Syntheses, analytical and X-ray structural data, AC susceptibility data.

Conflict of interest

There is no conflict to declare.

References

- X. Zhang, W. Wang, Z. Hu, G. Wang and K. Uvdal, Coordination polymers for energy transfer: Preparations, properties, sensing applications, and perspectives. *Coord. Chem. Rev.*, 2015, **284**, 206.
- L. R. Mingabudinova, V. V. Vinogradov, V. A. Milichko, E. Hey-Hawkins and A. V. Vinogradov, Metal-organic frameworks as competitive materials for non-linear optics, *Chem. Soc. Rev.*, 2016, **45**, 5408.
- A. Ovsyannikov, S. Solovieva, I. Antipin and S. Ferlay, Coordination Polymers based on calixarene derivatives: Structures and properties. *Coord. Chem. Rev.*, 2017, **352**, 151.
- O. Drath and C. Boskovic, Switchable cobalt coordination polymers: Spin crossover and valence tautomerism. *Coord. Chem. Rev.*, 2018, **375**, 256.
- N. Li, R. Feng, J. Zhu, Z. Chang and X.-H. Bu, Conformation versatility of ligands in coordination polymers: From structural diversity to properties and applications. *Coord. Chem. Rev.*, 2018, **375**, 558.
- W. P. Lustig and J. Li, Luminescent metal-organic frameworks and coordination polymers as alternative phosphors for energy efficient lighting devices. *Coord. Chem. Rev.*, 2018, **373**, 116.
- J.-K. Sun, X.-D. Yang, G.-Y. Yang and J. Zhang, Bipyridinium derivative-based coordination polymers: From synthesis to materials applications. *Coord. Chem. Rev.*, 2019, **378**, 533.

- 8 Q. Yue and E.-Q. Gao, Azide and carboxylate as simultaneous coupler for magnetic coordination polymers. *Coord. Chem. Rev.*, 2019, **382**, 1.
- 9 M. K. Bera, T. Mori, T. Yoshida, K. Ariga and M. Higuchi, Construction of Coordination Nanosheets Based on Tris(2,2'-bipyridine)-Iron (Fe²⁺) Complexes as Potential Electrochromic Materials. *ACS Appl. Mater. Interfaces*, 2019, **11**, 11893.
- 10 Y. Cheng, S. Deng, F. Sun and Y. H. Zhou, Synthesis of luminescent Cu₉S₅ nanoclusters from copper-2,5-dimercapto-1,3,4-thiadiazole coordination polymer as pH sensor. *J. Lumin.*, 2019, **210**, 38.
- 11 S. L. Hanna, X. Zhang, K. Otake, R. J. Drout, P. Li, T. Islamoglu and O.K. Farha, Guest-Dependent Single-Crystal-to-Single-Crystal Phase Transitions in a Two-Dimensional Uranyl-Based Metal–Organic Framework. *Cryst. Growth Des.*, 2019, **19**, 506.
- 12 Y.-S. Kang, Y. Lu, K. Chen, Y. Zhao, P. Wang and W.-Y. Sun, Metal–organic frameworks with catalytic centers: From synthesis to catalytic application. *Coord. Chem. Rev.*, 2019, **378**, 262.
- 13 J. Pan, D. Zhang, M.-M. Shang, Y. Mu, S.-D. Han and G.-M. Wang, An anionic Cd-based coordination polymer exhibiting ion-exchange behavior for photoluminescence and selective dye adsorption. *J. Lumin.*, 2019, **210**, 70.
- 14 J. Zhang, W. Kosaka, S. Kitagawa, M. Takata and H. Miyasaka, In Situ Tracking of Dynamic NO Capture through a Crystal-to-Crystal Transformation from a Gate-Open-Type Chain Porous Coordination Polymer to a NO-Adducted Discrete Isomer. *Chem. Eur. J.*, 2019, **25**, 3020.
- 15 X.-M. Zhang, P. Li, W. Gao, J.-P. Liu, Spin-canting magnetization in 3D metal organic frameworks based on strip-shaped Δ-chains. *RSC Adv.*, 2015, **5**, 76752.
- 16 J.-P. Zhao, C. Zhao, W.-C. Song, L. Wang, Y. Xie, J.-R. Li and X.-H. Bu, 4-Substituent pyridine directed cobalt(II) azides: solvothermal synthesis, structure, and magnetic properties. *Dalton Trans.*, 2015, **44**, 10289.
- 17 P. Manna, B. K. Tripuramallu, S. Bommakanti and S. K. Das, Synthesis, characterization and magnetism of metal–organic compounds: role of the positions of the coordinating groups of a meso-flexible ligand in placing anisotropy to exhibit spin-canting behavior. *Dalton Trans.*, 2015, **44**, 2852.
- 18 T. Gong, X. Yang, Q. Sui, Y. Qi, F.-G. Xi and E.-Q. Gao, Magnetic and Photochromic Properties of a Manganese(II) Metal-Zwitterionic Coordination Polymer. *Inorg. Chem.*, 2016, **55**, 96.
- 19 J.-Y. Tsao, J.-D. Tsai and C.-I. Yang, Azide-bridged Cu(II), Mn(II) and Co(II) coordination polymers constructed with a bifunctional ligand of 6-(1H-tetrazol-5-yl)-2,2'-bipyridine. *Dalton Trans.*, 2016, **45**, 3388.
- 20 R. Lescouëzec, L. M. Toma, J. Vaissermann, M. Verdager, F. S. Delgado, C. Ruiz-Pérez, F. Lloret and M. Julve, Design of single chain magnets through cyanide-bearing six-coordinate complexes. *Coord. Chem. Rev.*, 2005, **249**, 2691.
- 21 H.-L. Sun, Z.-M. Wang and S. Gao, Strategies towards single-chain magnets. *Coord. Chem. Rev.*, 2010, **254**, 1081.
- 22 W.-X. Zhang, T. Shiga, H. Miyasaka and M. Yamashita, New Approach for Designing Single-Chain Magnets: Organization of Chains via Hydrogen Bonding between Nucleobases. *J. Am. Chem. Soc.*, 2012, **134**, 6908.
- 23 W.-X. Zhang, R. Ishikawa, B. Breedlove and M. Yamashita, Single-chain magnets: beyond the Glauber model. *RSC Adv.*, 2013, **3**, 3772.
- 24 S. Wöhlert, Z. Tomkowicz, M. Rams, S. G. Ebbinghaus, L. Fink, M. U. Schmidt and C. Näther, Influence of the co-Ligand on the Magnetic and Relaxation Properties of Layered Cobalt(II) Thiocyanato Coordination Polymers. *Inorg. Chem.*, 2014, **53**, 8298.
- 25 S. Dhers, H. L.C. Feltham and S. Brooker, A toolbox of building blocks, linkers and crystallisation methods used to generate single-chain magnets. *Coord. Chem. Rev.*, 2015, **296**, 24.
- 26 J. Werner, Z. Tomkowicz, M. Rams, S. G. Ebbinghaus, T. Neumann and C. Näther, Synthesis, structure and properties of [Co(NCS)₂(4-(4-chlorobenzyl)pyridine)₂]_n, that shows slow magnetic relaxations and a metamagnetic transition. *Dalton Trans.*, 2015, **44**, 14149.
- 27 J. Werner, M. Rams, Z. Tomkowicz, T. Runčevski, R. E. Dinnebier, S. Suckert and C. Näther, Thermodynamically Metastable Thiocyanato Coordination Polymer That Shows Slow Relaxations of the Magnetization. *Inorg. Chem.*, 2015, **54**, 2893.
- 28 X.-B. Li, A.-L. Cheng and E.-Q. Gao, Random mixed-metal Co_{1-x}Ni_x single-chain magnets with simultaneous azide, carboxylate and tetrazolate bridges. *Dalton Trans.*, 2018, **47**, 9685.
- 29 E.-C. Yang, H.-S. Huang, S.-Y. Huang, S.-Y. Huang, Y.-Y. Chang, G.-H. Lee, H.-S. Sheu and C.-K. Chang, A one dimensional coordination polymer composed of antiferromagnetically coupled disk-like [Mn₇] units. *CrystEngComm*, 2018, **20**, 6963.
- 30 A. Kawamura, A. S. Filatov, J.S. Anderson and I.-R. Jeon, Slow Magnetic Relaxation of Co(II) Single Chains Embedded within Metal–Organic Superstructures. *Inorg. Chem.*, 2019, **58**, 3764.
- 31 A. Rodríguez-Diéguez, S. Pérez-Yáñez, L. Ruiz-Rubio, J. M. Seco, J. Cepeda, From isolated to 2D coordination polymers based on 6-aminonicotinate and 3d-metal ions: towards field-induced single-ion-magnets. *CrystEngComm*, 2017, **19**, 2229.
- 32 D. Shao, L. Shi, F.-X. Shen and X.-Y. Wang, A cyano-bridged coordination nanotube showing field-induced slow magnetic relaxation. *CrystEngComm*, 2017, **19**, 5707.
- 33 A. A. García-Valdivia, J. M. Seco, J. Cepeda and A. Rodríguez-Diéguez, Designing Single-Ion Magnets and Phosphorescent Materials with 1-Methylimidazole-5-carboxylate and Transition-Metal Ions. *Inorg. Chem.* 2017, **56**, 13897.
- 34 P. Mondal, B. Dey, S. Roy, S. Prasad Bera, R. Nasani, A. Santra and S. Konar, Field-Induced Slow Magnetic Relaxation and Anion/Solvent Dependent Proton Conduction in Cobalt(II) Coordination Polymers. *Cryst. Growth Des.* 2018, **18**, 6211.
- 35 X. Ma, Y. Liu, W. Song, Z. Wang, X. Liu, G. Xie, S. Chen and S. Gao, A difunctional azido-cobalt(II) coordination polymer exhibiting slow magnetic relaxation behaviour and high-energy characteristics with good thermostability and insensitivity. *Dalton Trans.* 2018, **47**, 12092.
- 36 X. Hou, X. Wang, X. Liu, J. Wang, L. Tang and P. Ju, Fine-tuning the effects of auxiliary ligands on two trigonal-bipyramid cobalt(II) complexes exhibiting field-induced slow magnetic relaxation. *New J. Chem.*, 2018, **42**, 8583.
- 37 L. Shi, F.-X. Shen, D. Shao, Y.-Q. Zhang and X.-Y. Wang, An *ab initio* molecular dynamics method for cocrystal prediction: validation of the approach. *CrystEngComm*, 2019, **21**, 3176.
- 38 R. Robson, Design and its limitations in the construction of bi- and poly-nuclear coordination complexes and coordination polymers (aka MOFs): a personal view. *Dalton Trans.*, 2008, 5113.
- 39 V. R. Pedireddi and S. Varughese, Solvent-Dependent Coordination Polymers: Cobalt Complexes of 3,5-Dinitrobenzoic Acid and 3,5-Dinitro-4-methylbenzoic Acid with 4,4'-Bipyridine. *Inorg. Chem.*, 2004, **43**, 450.
- 40 A. Y. Robin and K. M. Fromm, Coordination polymer networks with O- and N-donors: What they are, why and how they are made. *Coord. Chem. Rev.*, 2006, **250**, 2127.
- 41 M. Du, C.-P. Li, C.-S. Liu and S.-M. Fang, Design and

- construction of coordination polymers with mixed-ligand synthetic strategy. *Coord. Chem. Rev.*, 2013, **257**, 1282.
- 42 K.T. Mahmudov, M. N. Kopylovich, M. F. C. Guedes da Silva and A. J.L. Pombeiro, Non-covalent interactions in the synthesis of coordination compounds: Recent advances, *Coord. Chem. Rev.*, 2017, **345**, 54.
- 43 W.-W. He, S.-L. Li and Y.-Q. Lan, Liquid-free single-crystal to single-crystal transformations in coordination polymers. *Inorg. Chem. Front.*, 2018, **5**, 279.
- 44 X. Zhang, H. Chen, B. Li, G. Liu and X. Liu, Construction of functional coordination polymers derived from designed flexible bis(4-carboxybenzyl)amine. *CrystEngComm*, 2019, **21**, 1231.
- 45 S. R. Marshall, C.D. Incarvito, J. L. Manson, A. L. Rheingold and J. S. Miller, Synthesis, Structure, and Magnetic Properties of $\text{Co}_2\{\text{N}(\text{CN})_2\}_4\text{bpym}\cdot\text{H}_2\text{O}$ and $\text{M}\{\text{N}(\text{CN})_2\}_2\text{bpym}\cdot\text{H}_2\text{O}$ (M = Mn, Fe, Co; bpym = 2,2'-Bipyrimidine). *Inorg. Chem.*, 2000, **39**, 1969.
- 46 S. R. Batten and K. S. Murray, Structure and magnetism of coordination polymers containing dicyanamide and tricyanomethanide. *Coord. Chem. Rev.*, 2003, **246**, 103.
- 47 P. M. van der Werff, S. R. Batten, P. Jensen, B. Moubaraki, K. S. Murray and J. D. Cashion, Structure and Magnetism of 3D Anionic Metal Dicyanamide ($\text{MePh}_3\text{P}\}\text{M}(\text{dca})_3$) (M = Fe, Co, Ni) and ($\text{EtPh}_3\text{P}\}\text{M}(\text{dca})_3$) (M = Mn, Co, Ni) Networks. *Cryst. Growth Des.*, 2004, **4**, 503.
- 48 H.-L. Sun, Z.-M. Wang and S. Gao, Synthesis, Crystal Structures, and Magnetism of Cobalt Coordination Polymers Based on Dicyanamide and Pyrazine-dioxide Derivatives. *Inorg. Chem.*, 2005, **44**, 2169.
- 49 F. A. Mautner, M. Traber, R. C. Fischer, S.S. Massoud and R. Vicente, Synthesis, crystal structures, spectral and magnetic properties of 1-D polymeric dicyanamido-metal(II) complexes. *Polyhedron*, 2017, **138**, 13.
- 50 J. L. Manson, C. R. Kmetz, Q. Z. Huang, J. W. Lynn, G. M. Bendele, S. Pagola, P. W. Stephens, L. M. Liable-Sands, A. L. Rheingold, A. J. Epstein and J. S. Miller, Spin Canting in the 3D Anionic Dicyanamide Structure ($\text{SPh}_3\text{Mn}(\text{dca})_3$) (Ph = Phenyl, dca = Dicyanamide). *Chem. Mater.*, 1998, **10**, 2552.
- 51 S. R. Batten, P. Jensen, B. Moubaraki, K. S. Murray and R. Robson, Structure and molecular magnetism of the rutile-related compounds $\text{M}(\text{dca})_2$, M = Co^{II} , Ni^{II} , Cu^{II} , dca = dicyanamide, $\text{N}(\text{CN})_2^-$. *Chem. Commun.*, 1998, 439.
- 52 M. Kurmoo and C. J. Kepert, Hard magnets based on transition metal complexes with the dicyanamide anion, $\{\text{N}(\text{CN})_2\}^-$. *New J. Chem.*, 1998, **22**, 1515.
- 53 C. R. Kmetz, J. L. Manson, Q. Z. Huang, J. W. Lynn, R. W. Erwin, J. S. Miller and A. J. Epstein, Magnetic Phase Transitions in $\text{M}^{\text{II}}[\text{N}(\text{CN})_2]_2$. *Mol. Cryst. Liquid Cryst.*, 1999, **334**, 631.
- 54 C. R. Kmetz, Q. Z. Huang, J. W. Lynn, R. W. Erwin, J. L. Manson, S. McCall, J. E. Crow, K. L. Stevenson, J. S. Miller and A. J. Epstein, Noncollinear antiferromagnetic structure of the molecule-based magnet $\text{Mn}[\text{N}(\text{CN})_2]_2$. *Phys. Rev. B*, 2000, **62**, 5576.
- 55 J. L. Manson, C. R. Kmetz, F. Palacio, A. J. Epstein and J. S. Miller, Low-Field Remanent Magnetization in the Weak Ferromagnet $\text{Mn}[\text{N}(\text{CN})_2]_2$. Evidence for Spin-Flop Behavior. *Chem. Mater.*, 2001, **13**, 1068.
- 56 A. Świtlicka-Olszewska, J. Palion-Gazda, T. Klemens, B. Machura, J. Vallejo, J. Cano, F. Lloret and M. Julve, Single-ion magnet behavior in mononuclear and two-dimensional dicyanamide-containing cobalt(II) complexes. *Dalton Trans.*, 2016, **45**, 10181.
- 57 J. Palion-Gazda, T. Klemens, B. Machura, J. Vallejo, F. Lloret and M. Julve, Single ion magnet behavior in a two-dimensional network of dicyanamide-bridged cobalt(II) ions. *Dalton Trans.*, 2015, **44**, 2989.
- 58 R. Sen, A. Bhattacharjee, P. Gütllich, Y. Miyashita, K.-I. Okamoto and S. Koner, Structural and magnetic diversity in metal-dicyanamido polymer moieties: Paramagnetic and antiferromagnetic 1D chain compound and weakly ferromagnetic 2D motif. *Inorg. Chim. Acta*, 2009, **362**, 4663.
- 59 A. Das, C. Marschner, J. Cano, J. Baumgartner, J. Ribas, M. S. El Fallah and S. Mitra, Synthesis, crystal structures and magnetic behaviors of two dicyanamide bridged di- and polynuclear complexes of cobalt(II) derived from 2,4,6-tris(2-pyridyl)1,3,5-triazine and imidazole. *Polyhedron*, 2009, **28**, 2436.
- 60 A. Das, B. Bhattacharya, D. K. Maity, A. Halder and D. Ghoshal, Construction of five dicyanamide based coordination polymers with diverse dimensionality: Synthesis, characterization and photoluminescence study. *Polyhedron*, 2016, **117**, 585.
- 61 Oxford Diffraction, CrysAlis PRO, Oxford Diffraction Ltd, Yarnton, England, 2011.
- 62 G. M. Sheldrick, Crystal structure refinement with SHELXL. *Acta Crystallogr., Sect. C: Struct. Chem.*, 2015, **71**, 3.
- 63 A. Hassan, L. Pardi, J. Krzystek, A. Sienkiewicz, P. Goy, M. Rohrer and L.-C. Brunel, Ultrawide Band Multifrequency High-Field EMR Technique: A Methodology for Increasing Spectroscopic Information, *J. Magn. Reson.*, 2000, **142** (2), 300.
- 64 G. A. Bain and J. F. Berry, Diamagnetic Corrections and Pascal's Constants, *J. Chem. Ed.*, 2008, **85**, 532.
- 65 J. Carranza, J. Sletten, F. Lloret and M. Julve, Structural analysis and magnetic properties of the copper(II) dicyanamide complexes $[\text{Cu}_2(\text{dmphen})_2(\text{dca})_4]$, $[\text{Cu}(\text{dmphen})(\text{dca})(\text{NO}_3)]_n$ and $[\text{Cu}(4,4'\text{-dmbpy})(\text{H}_2\text{O})(\text{dca})_2]$ (dca=dicyanamide; dmphen=2,9-dimethyl-1,10-phenanthroline; 4,4'-dmbpy=4,4'-dimethyl-2,2'-bipyridine). *Inorg. Chim. Acta*, 2004, **357**, 3304.
- 66 F. A. Mautner, M. Traber, R. C. Fischer, S. S. Massoud and R. Vicente, Synthesis, crystal structures, spectral and magnetic properties of 1-D polymeric dicyanamido-metal(II) complexes. *Polyhedron*, 2017, **138**, 13.
- 67 A. B. P. Lever, *Inorganic Electronic Spectroscopy*, Elsevier, Amsterdam, 1984.
- 68 J.M. Herrera, A. Bleuzen, Y. Dromzée, M. Julve, F. Lloret and M. Verdager, Crystal Structures and Magnetic Properties of Two Octacyanotungstate(IV) and (V)-Cobalt(II) Three-Dimensional Bimetallic Frameworks. *Inorg. Chem.*, 2003, **42**, 7052.
- 69 A. Mašlejová, S. Uhrinová, J. Mrozinski, B. Zurowska, M. C. Munoz and M. Julve, Study of the mutual influence of ligands in cobalt(II) complexes containing thiocyanate and imidazole derivatives. *Inorg. Chim. Acta*, 1997, **255**, 343.
- 70 S. Roy, S. Choubey, K. Bhar, N. Sikdar, J. Sánchez Costa, P. Mitra and B. Kumar Ghosh, Counter anion dependent gradual spin transition in a 1D cobalt(II) coordination polymer. *Dalton Trans.*, 2015, **44**, 7774.
- 71 W. Huang, J. Zhang and C. Zhang, *catena*-Poly[[bis(4-methylpyridine-*j*N)-cobalt(II)]-di- μ -dicyanamido- $\kappa^2\text{N}^1:\text{N}^5$]. *Acta Cryst.*, 2013, **E69**, m90.
- 72 L.-L. Zheng and X.-M. Zhuang, Syntheses, Crystal Structures and Magnetism of Three Metal-Dicyanamide Coordination polymers with Isonicotinamide Ligand, *Z. Anorg. Allg. Chem.*, 2010, **636**, 2500.
- 73 Q. Bao, Y. Ma, Q. Zhao, Y. Luo and B. Sun, Two new one-dimensional coordination polymers containing $[\text{N}(\text{CN})_2]^-$ —Syntheses, structures, and magnetic properties of $[\text{M}^{\text{II}}(3\text{-Bzpy})_2(\text{N}(\text{CN})_2)_2]$ (M = Mn (1) and Co (2) and 3-Bzpy = 3-benzoylpyridine). *Can. J. Chem.*, 2012, **90**, 362.
- 74 M. Wriedt and C. Näther, Directed synthesis of μ -1,3,5 bridged dicyanamides by thermal decomposition of μ -1,5 bridged precursor compounds. *Dalton Trans.*, 2011, **40**, 886.

- 75 V.A. Blatov, Nanocluster analysis of intermetallic structures with the program package TOPOS. *Struct. Chem.*, 2012, **23**, 955.
- 76 R. Boča, *Program MIF&FIT*. University of SS Cyril and Methodius, Trnava, 2019.
- 77 S. Stoll and A. Schweiger, Easy Spin, a comprehensive software package for spectral simulation and analysis in EPR *J. Magn. Reson.* 2006, **178(1)**, 42.
- 78 R. Boča, *Struct. Bonding*, 2006, **117**, 1.
- 79 A. Abragam and B. Bleaney, *Electron Paramagnetic Resonance of Transition Ions*. Clarendon Press, Oxford, 1970.
- 80 K.J. Standley and R.A. Vaughan, *Electron Spin Relaxation Phenomena in Solids*, Plenum Press, New York, 1969.
- 81 P.L. Scott and C.D. Jeffries, Spin-Lattice Relaxation in Some Rare-Earth Salts at Helium Temperatures; Observation of the Phonon Bottleneck. *Phys. Rev.* 1962, **127**, 32.
- 82 L. Tesi, A. Lunghi, M. Atzori, E. Lucaccini, L. Sorace, F. Totti and R. Sessoli, Giant spin-phonon bottleneck effects in evaporable vanadyl-based molecules with long spin coherence. *Dalton Trans.* 2016, **45**, 16635.
- 83 E. Rousset, M. Piccardo, R. W. Gable, A. Soncini, C. Boskovic, M. E. Boulon and L. Sorace, Slow Magnetic Relaxation in Lanthanoid Crown Ether Complexes: Interplay of Raman and Anomalous Phonon Bottleneck Processes. *Chemistry – An European Journal*, 2018, **24**, 14768.
- 84 R. Boča, C. Rajnák, J. Moncol, J. Titiš and D. Valigura, Breaking the Magic Border of One Second for Slow Magnetic Relaxation of Cobalt-Based Single Ion Magnets. *Inorg. Chem.* 2018, **57**, 14314.
- 85 R. Boča and C. Rajnák, Unexpected behavior of single ion magnets. *Coord. Chem. Rev.*, 2021, **430**, 213657.
- 86 C. Rajnák and R. Boča, Reciprocating thermal behavior in the family of single ion magnets. *Coord. Chem. Rev.*, 2021, **436**, 213808.
- 87 A. Świtlicka, B. Machura, R. Kruszyński, N. Moliner, J. M. Carbonell, J. Cano, F. Lloret and M. Julve, Magneto-structural diversity of Co(II) compounds with 1-benzylimidazole induced by linear pseudohalide coligands, *Inorg. Chem. Front.*, 2020, **7**, 4535.
- 88 A. Świtlicka, J. Palion-Gazda, B. Machura, J. Cano, F. Lloret and M. Julve, Field-induced slow magnetic relaxation of pseudooctahedral cobalt(II) complexes with positive axial and large rhombic anisotropy, *Dalton Trans.*, 2019, **48**, 1404.